Deformation and mechanics of a pulvinus-inspired material

Loïc Tadrist, Younes Mammadi, Julien Diperi, Jean-Marc Linares

Deformation and mechanics of a pulvinus-inspired material

Loïc Tadrist, Younes Mammadi, Julien Diperi and Jean-Marc Linares

Aix-Marseille Université, CNRS, ISM, Marseille, France

E-mail: loic.tadrist@univ-amu.fr

February 2022

Abstract. Mimosa Pudica rapidly folds leaves when touched. Motion is created by pulvini, "the plant muscles" that allow plants to produce various complex motion. Plants rely on local control of the turgor pressure to create on-demand motion. In this paper, the mechanics of a cellular material inspired from pulvinus of Mimosa Pudica is studied. First, the manufacturing process of a cell-controllable material is described. Its deformation behaviour when pressured is tested, focussing on 3 pressure patterns of reference. The deformations are modelled based on the minimisation of elastic energy framework. Depending on pressurisation pattern and magnitude, reversible buckling-induced motion may occur.

Keywords: Pneumatic cellular material, Deformations, Pulvinus, Bioinspiration, Biomimetics

Submitted to: *Bioinspir. Biomim.*

1. Introduction: Drawing inspiration from nature for versatile and resilient actuators

The interest for bioinspired actuator is growing because of their adaptability and controllability for application to soft robotics. New designs are proposed every year. The first pneumatic muscle was patented by Alexandre-Henri Morin (Morin 1951, Morin 1953, Hannaford & Winters 1990) and adapted by Joseph Laws McKibben to allow his polio-paralysed girl Karan to move her arm (Gurstelle 2017). This reference device is now known as the McKibben pneumatic muscle. Skeletal muscle has also been mimicked with different pneumatic technology (Villegas et al. 2012) but also with electro-active polymers (EAP), shape memory alloys (SMA), piezoelectric actuators, dielectric elastomer (DEA), ionic polymer metal composite (IPMC), coiled polymers, etc (Zhang et al. 2019). Some bio-inspired muscles simply mimic the linear motion created by a striated muscle or its external shape (*e.g.* McKiben muscle) whereas more sophisticated ones copy its multi-scale structure or its working behaviour (Higueras-Ruiz et al. 2021).

Similarly to the animal muscle, pulvinus (the "plant muscle") has triggered lots of bioinspired devices with hydrogels (Xu et al. 2021) or fluid pressure as the actuation source, with gas (Vasista & Tong 2012, Li & Wang 2015*b*, Li & Wang 2015*a*, Li & Wang 2016) or liquid osmosis (Piyasena et al. 2009, Must et al. 2019).

Most of plants equipped with pulvini are able to produce a large variety of motion. They open leaves during the day, track sun light to maximize collection of energy, and fold leaves at night for protection. However, some plants have more refined opening strategies. For instance, Mimosa Pudica folds leaves when touched to reduce predation from herbivores whereas Samanean Saman folds leaves at night or on cloudy days to prevent the rain being intercepted by the foliage. Mimosa pudica has been appealing for biomimetism because its motion time-scale is in the order of a second (Dumais & Forterre 2012). However, most of the plants are able to move slowly either during growth or by swelling (Forterre 2013).

In Mimosa Pudica, pulvini are found at 3 locations: at the base of the petiole, at the base of the rachis and at the base of each leaflet as shown in Figure 1a. Pulvini respond to a mechanical stimulus depending on its intensity: when gently touched, it only folds few leaflets near the contact whereas a strong impact creates the folding of the whole leaf with the actuation of all leaflets, rachis and petiole pulvini.

A simplified pulvinus cross section is drawn in Figure 1b. The pulvinus is organised around a dense core of vascular tissues (xylem and phloem) that allows water and sieve transport. This core is surrounded by spherical pachenchyma cells of diameter $15\,\mu\text{m} < a < 30\,\mu\text{m}$ and thickness $0.75\,\mu\text{m} < t < 3\,\mu\text{m}$ (Fleurat-Lessard & Millet 1984). Those motor cells deform under turgor pressure and create motion.

Pulvinus are encountered in plants of distinct origins among angiosperms, see Figure

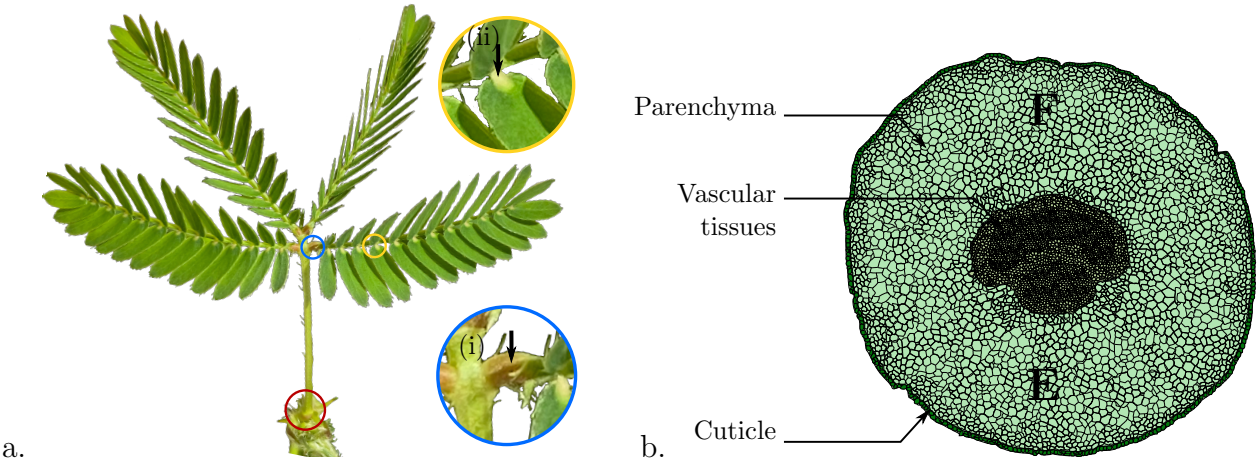

Figure 1. a. Open leaf of Mimosa pudica with pulvini locations. Petiole pulvinus: red circle. Rachis pulvinus: blue circle. Leaflet pulvinus: yellow circle. Inset (i): close-up on rachis and leaflet petiole. Inset (ii): Closed leaf. b. Scheme of cross section of pulvinus with parenchyma cells (green shade), cuticule layer (thick black), lignified vascular tissues: phloem and xylem. E: Extensor. F: Flexor.

2. Most thigmonastic plants (sensitive to touch, more generally to mechanical stimulation) are from Oxalidaceae and fabaceae families (Eudicots) but pulvinus are also found in distant families such as Marantaceae family (monocots, not thigmonastic), see Figure 2. A similar actuation principle is used to rapidly and reversibly move stamen filaments of flowers of some plants of the Berberidaceae and Cactaceae families (e.g. Berberis Canadensis, Opuntia polyacantha). These motions are used to promote pollen transfer to a visiting insect and/or to prevent pollen robbing.

Thigmonastic pulvini, nyctinastic pulvini and thigmonastic stamens have different functions and originate from completely different developmental steps. Currently, it is unknown if sensitive stamens filaments and pulvini originate from a common ancestor of if they are an example of convergent evolution. However, the actuation mechanism (local change of turgor pressure by osmosis) seems robust among plant reign for rapid and slow motions. The convergent or highly preserved evolution of pulvinus (or pulvinus-like actuation mechanism) makes it an excellent source of inspiration to create new kind of actuator that can produce various complex motions.

We hypothesise that the multi-scale structure of pulvinus, provides it with interesting mechanical properties such as on-demand anisotropy, on demand stiffness and on-demand complex motion.

Testing this hypothesis requires building a material that is controllable at the cellular level. In the first part of the paper, we leverage on existing pneumatic actuators (Shepherd et al. 2011, Siéfert et al. 2019) to build a cell-controllable meta-material inspired from

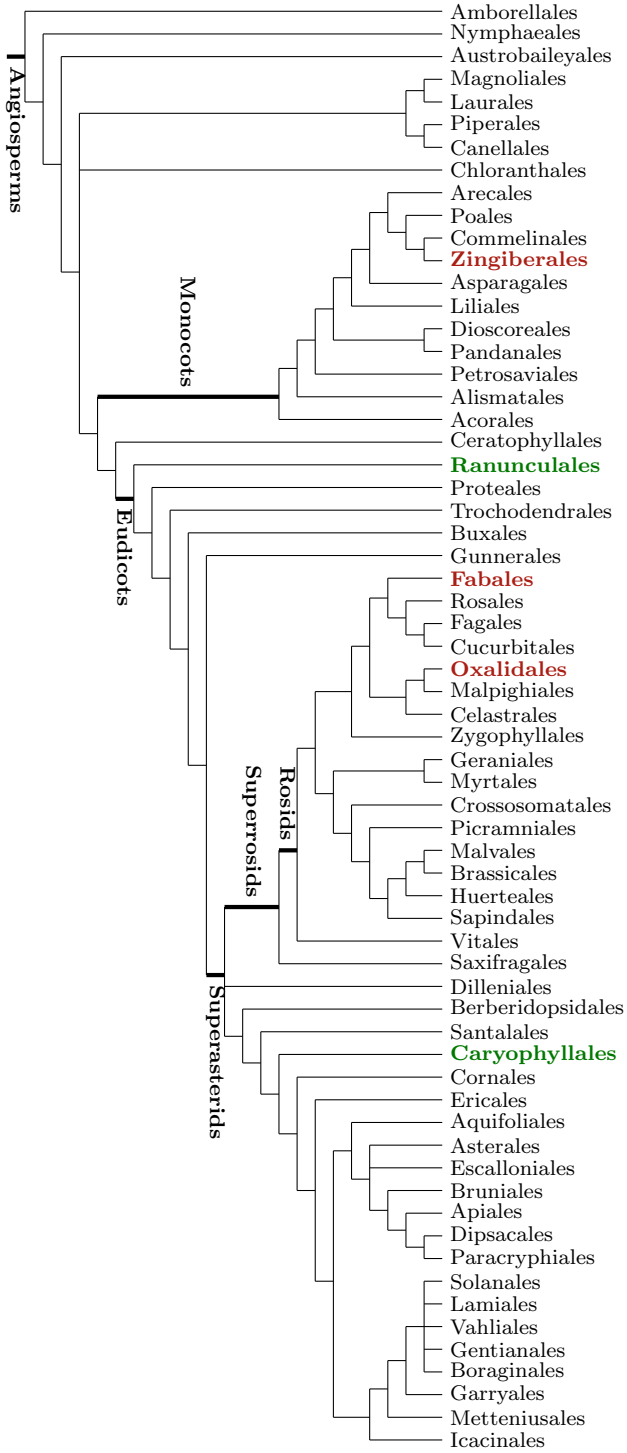

Figure 2. Phylogenetic tree form angiosperms, the "flowering plants", from plants reign, (Plantae → Tracheophyta → Angiosperms), adapted from The Angiosperm Phylogeny Group (APG IV 2016). Main families with pulvinus equiped plants are marked in dark red: Zingiberales→Marantaceae (e.g. the prayer plant - Maranta leuconeura, not thigmonastic), Oxalidales→Oxalidaceae (e.g. Oxalis hedysaroides) and Fabales→Fabaceae (e.g touch-me-not - Mimosa Pudica) families. Plants with excitable stamen filaments are marked in dark green: Ranunculales→Berberidaceae (e.g. Berberis Canadensis (Fleurat-Lessard & Millet 1984)), Caryophyllales→Cactaceae(e.g. Opuntia polyacantha (Cota-Sánchez et al. 2013))

Parameter		Value
Young's Modulus	E	P1: 18 kPa; P2: 9 kPa
Poisson ration	ν	$\simeq 0.43$[1]

Table 1. Mechanical properties of the material used to create the biomimetic pulvinus material. P1: Prototype 1. P2: Prototype 2. [1] from (Boonvisut & Çavuşoğlu 2012)

pulvinus. In the second part, we test the deformations of the material when pressurised depending on pressure level and the chosen pattern. We then rationalize the observation based on a minimisation on elastic energy model and give the first insights on the mechanical behaviour of this meta-material. Finally, we discuss our findings regarding possible uses of such a meta-material.

2. Material and Methods: Cell-controllable pneumatic pulvinus

The biomimetic pulvinus is a cellular material made of soft silicone material (Ecoflex 00-50; *Smooth-On, Inc.*). Two prototypes were manufactured with identical dimensions but different Young's moduli, see Table 1. Young moduli were measured on a self-weight bending experiment. To be able to control the material a two different scales, each cell is air-impermeable and its inner pressure may be externally controlled. Air pressure is provided by the pressured-air system of the lab and finely controlled thanks to a pressure reducer.

2.1. Prototype design and manufacturing

Moulds were created using computer aided design with parametrized dimensions (3D Experience, *Dassault systemes*). The cell inner dimension a, the thickness t and the number of cells N were adjustable on the CAD software. The moulds were 3D printed (Flex93 Ultra, *Volumic*) with a thickness of 2 mm, see Figure 3b. The moulds were soft enough to permit silicone casting and easy unmoulding.

Each half of the prototype has been moulded with Ecoflex 50-00 from Smooth-On, Inc. with a 1:1 ratio. Mixing ratio was accurately measured by weighting with a precise scale. Mixing was done by stirring vigorously which introduced air bubbles. Air bubbles were removed with a vacuum pump. Casting was realised by carefully pouring the silicone to avoid detrimental air bubbles.

Curing was approximately 4 hours at ambient temperature. After complete curing, the two halves of the prototypes were glued together with a thin layer of silicone Ecoflex 50-00 and again cured for 4 hours.

Pneumatic feeding was done with silicone tubes of internal diameter 0.5 mm and external diameter 1.5 mm. Each tube was airtight pinched in a different cell. Pneumatic tubing was

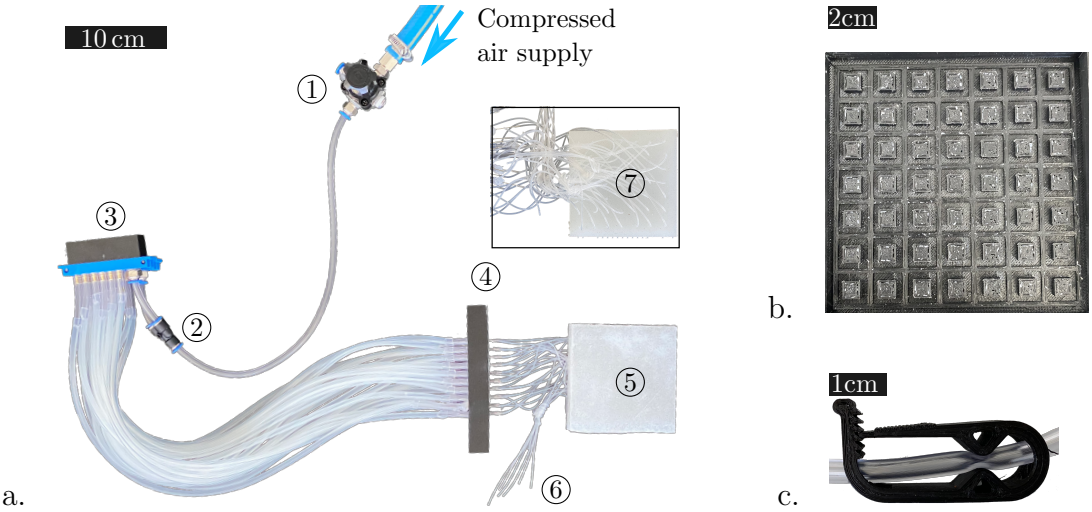

Figure 3. Prototype molding and assembly. a. Pneumatic prototype. The air is supplied by the lab air compression system.① Pressure reducer. ② flow divider to feed ③ multi-outlets distributors. ④ Macro-to-micro tubing interface. ⑤ Cellular material. ⑥ Unused cell inlets. ⑦ Reverse face of the prototype. b. 3D-printed mould with positive half cells. c. Manual valve for unique cell.

linked to the pressurized air system of the lab through a pressure reducer and multi-outlet distributors to allow controlling finely the pressure, Figure 3a. 3D printed manual valves allowed to turn on and off each cell independently to change the pattern of activated cells, Figure 3c. The present prototype was made with 7×7 cells with thick walls (inner cell dimension a =7 mm and thickness t =7 mm, see Figure 7). The total dimension of the pulvinus like piece was $105 \times 105 \times 21$ mm.

Pneumatic inflation and silicone casting techniques were chosen for simplicity and maintenance ease. Minimal external diameters of commercial silicone tubes usually range in few hundreds of microns. Cell dimensions (few milimeters) were chosen much larger than minimal commercial tubing dimensions (few hundreds of microns) to inflate cell without deforming much the tubes. Finally, silicone Young's modulus was chosen to match pulvinus growth ability (doubling dimension when inflated).

2.2. Measurement of the deformation field

Pulvinus-like material deformations were measured using a stereo-imaging digital image correlation set-up (DIC standard 3D, *Dantec dynamics*). One side of the cellular material was prepared by finely spraying black paint to create a synthetic Schlieren for image correlation. Stereo imaging was done with two cameras with a slight angle ($\simeq 6.65^o$) with the viewing direction.

Cellular material dimensions		Material parameters	
a	Cell inner dimension	E	Young Modulus
t	Cell wall thickness	ν	Poisson ratio
N	Number of cells on a line	Mechanical modelling	
V	Fluid volume of a cell	k	strain in extension
Experimental variables		k_t	strain in compression
P (P_0)	Fluid pressure (initial pressure)	$\mathcal{E}$	Total elastic energy
$\Delta P = P - P_0$	Applied pressure	$\mathcal{E}_f, \mathcal{E}_e, \mathcal{E}_c$	Face, edge and corner elastic energy
$\varepsilon_{xx}, \varepsilon_{yy}$	Measured surface strain	$\underline{\underline{\varepsilon}}$	Strain tensor
		$\underline{\underline{\sigma}}$	Stress tensor

Table 2. Table of parameters. P_0, V_0 indicate atmospheric pressure and initial fluid volume inside the cell. $\tilde{P}$ and $\tilde{\mathcal{E}}$ indicates dimensionless pressure and elastic energy.

Thin and long pipelines increase the hydraulic resistance of the prototype which has a typical response time of few seconds. During the experiment, images were taken some tens of seconds after pressure stabilized.

3. Mechanics of a cellular material

3.1. Deformations of a cellular material: experiments

3 inflation patterns have been tested. The first one is chequerboard (Figure 4a). The second is the anisotropic linear pattern (Figure 4b). The third is simply the pressurisation of 5x5 cells in the center of the cellular material (Figure 4c). To avoid edge effects, the outermost cells were let at nil pressure. For the three patterns, the pressure has been set equal for all cells but changed in magnitude. The different deformation fields are drawn in Figure 4 in the x and y directions depending on applied pressure. The amplitude of the measured strains increases with inflation pressure.

Those 3 patterns were chosen as references. The chequerboard pattern and the 5x5 centred cells create isotropic stress in the material whereas the linear pattern is anisotropic and create selective expansion. The chequerboard pattern and 5x5 centred cells allow to test the effect of pressure in neighbouring cells.

For the chequerboard pattern, the strains ε_{xx} and ε_{yy} focuses on pressured cells (Figure 4a). Differently, the linear anisotropic pattern shows nice stripes for ε_{xx} in the y-direction (Figure 4b). The presence of the cell wall is not observed in this direction and strains seem behaving collectively. The ε_{yy} strain shows separate cells with the wall between two adjacent pressured cells compressed, similarly to the chequerboard pattern. Finally, the 5x5 centered cells pattern shows stripes of large magnitude strains ε_{xx} in the y-direction and ε_{yy} in the x-directions (Figure 4c).

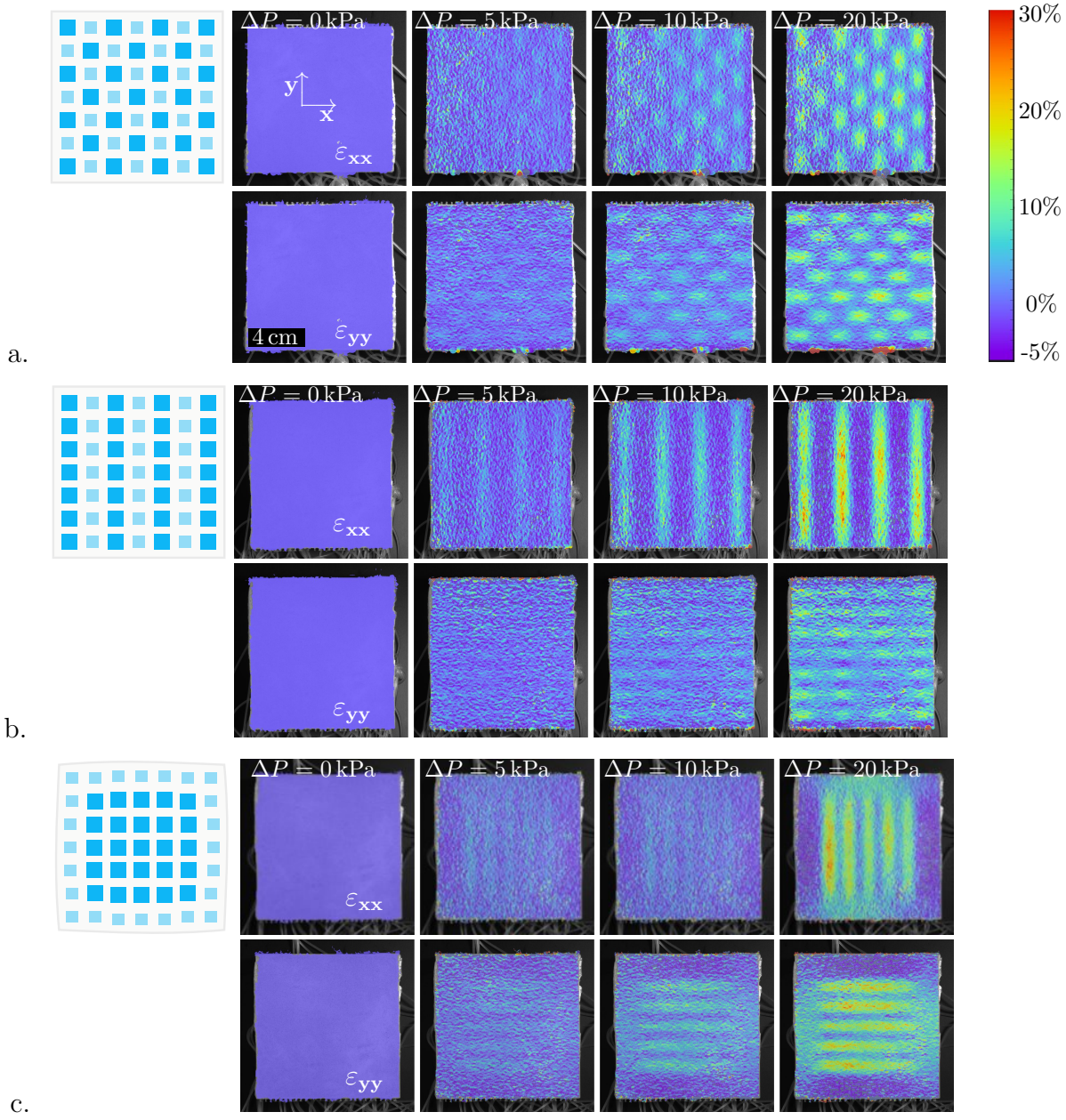

Figure 4. Pressurisation patterns of reference with corresponding main deformations at the surface of Prototype 1 (top: ε_{xx}, bottom: ε_{yy}). a. Pressured cells at the center. b. Chequerboard pattern c. Linear anisotropic pattern.

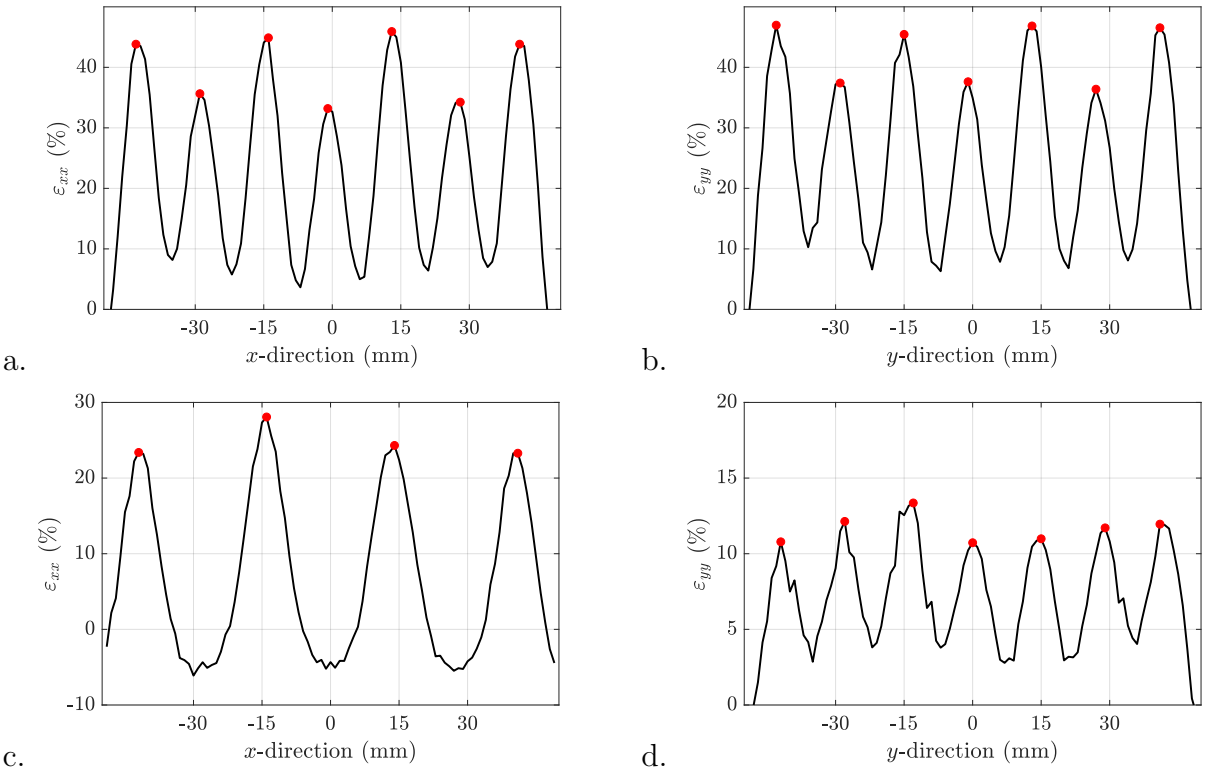

Figure 5. Example of deformation of the cellular material measured at the surface for a pressure ΔP =28 kPa. a and c. ε_{xx} averaged over the y-direction (a. Chequerboard pattern, Prototype 2. c. Anisotropic pattern, Prototype 1). b. and d. ε_{yy} averaged over the x-direction. (b. Chequerboard pattern, Prototype 2 d. Anisotropic pattern, Prototype 1). The peaks correspond to the center of cells where the material is stretched whereas the hollow correspond to walls where less stretching occurs.

The stripped pattern has been analysed by averaging the deformation value along the invariant direction (ε_{xx} in the y direction and ε_{yy} in the x-direction). Results for prototype 2 (P=28 kPa, chequerboard pattern), are plotted in figure 5a and b, and prototype 1 (P=28 kPa, anisotropic pattern), are plotted in figure 5c and d, for x and y-directions respectively.

The difference between successive maxima for the chequerboard pattern is due to the fact that the average is done over 3 or 4 pressured cells depending on the considered line. To correct this effect, each peak value must be adjusted by the number of cells, $N = 7$, divided by the number of pressured cells in the line, N_{press}, $N\ \varepsilon(\text{peak})/N_{\text{press}}$. Mean values of maximal deformations above the empty part of the cell (red points) are used to define the maximal stretching,

$$\max(\varepsilon_{xx}) = \frac{1}{N_{\text{peaks}}} \sum \frac{N}{N_{\text{press}}} \varepsilon_{xx}(\text{peak}) \quad \text{and} \quad \max(\varepsilon_{yy}) = \frac{1}{N_{\text{peaks}}} \sum \frac{N}{N_{\text{press}}} \varepsilon_{yy}(\text{peak}). \qquad (1)$$

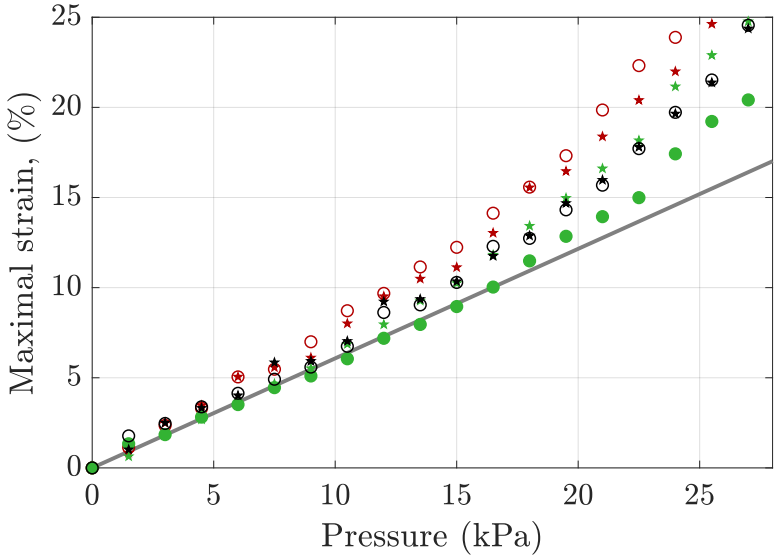

Figure 6. Evolution of maximal stretching and minimal stretching of the cellular material (Prototype 1). ⋆: $\max(\varepsilon_{xx})$. •: $\max(\varepsilon_{yy})$. Black: Chequerboard pattern. Green: Linear anisotropic pattern. Red: 5x5 centered cells pattern.

The variations of $\max(\varepsilon_{xx})$ (stars) and $\max(\varepsilon_{yy})$ (circles) are plotted as a function of inflation pressure, for prototype 1 for the 3 considered patterns in Figure 6. All are positive and increase non-linearly with inflation pressure when strains are larger than 10%. The values of ε_{xx} and ε_{yy} are similar for each pressure pattern. The differences between patterns are due to small collective effects.

3.2. Deformations of a cellular material: modelling

We consider a cellular material made of fluid-filled cells of dimension a embedded in an elastic material of thickness t, see Figure 7. A quasi-static approach is developed by elastic energy minimization.

The fluid volume of an undeformed cell is $V_0 = a^3$. This volume is surrounded by 6 square faces of volume a^2t, 12 edges of volume at^2 and 8 corners of volume t^3 of elastic material. Each face is shared by 2 cells, each edge is shared by 4 cells, and each corner is shared by 8 cells. The total volume of one cell is thus $v_{\text{cell}} = a^3 + 6a^2t/2 + 12at^2/4 + 8(t/2)^3 = (a+t)^3$.

When inflated, we suppose that the cell expansion is isotropic. The elastic energies of one face, one edge and one corner are computed. Then, similarly to cell volume, cell energy is determined by balancing face/edge/corner energies by the number of elements divided by the sharing coefficient.

A face of the cell is compressed in its normal direction and stretched in its plane. An

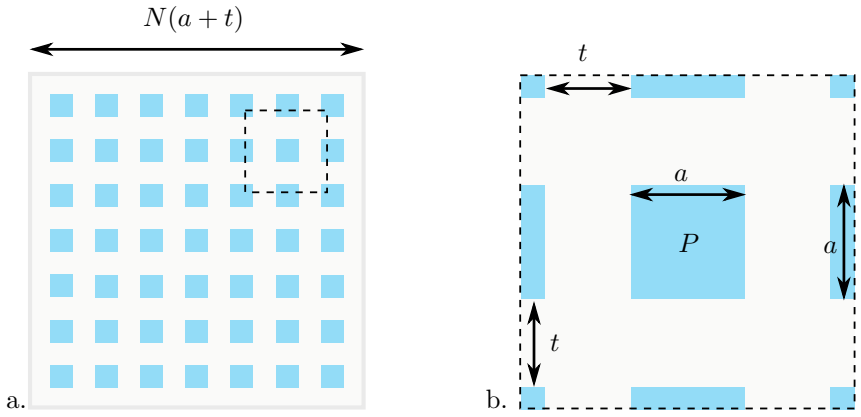

Figure 7. a. Schematic view of the cross section of the cellular material of dimension $N(a+t)+t$ b. close-up on one cell with inner dimension a and thickness t.

edge is stretched in its main direction and compressed in the two others. Finally, a corner in compressed in its 3 directions. The linearised deformation tensors of a face, an edge and a corner reads,

$$\underline{\underline{\varepsilon}}_{\mathrm{f}} = \begin{pmatrix} k & 0 & 0 \\ 0 & k & 0 \\ 0 & 0 & k_t \end{pmatrix}, \quad \underline{\underline{\varepsilon}}_{\mathrm{e}} = \begin{pmatrix} k & 0 & 0 \\ 0 & k_t & 0 \\ 0 & 0 & k_t \end{pmatrix} \quad \text{and} \quad \underline{\underline{\varepsilon}}_{\mathrm{c}} = \begin{pmatrix} k_t & 0 & 0 \\ 0 & k_t & 0 \\ 0 & 0 & k_t \end{pmatrix}. \tag{2}$$

As a first approximation, the elastic material is described by a linear Hook's law,

$$\underline{\underline{\sigma}} = \frac{E}{1+\nu}\underline{\underline{\varepsilon}} + \frac{\nu E}{(1+\nu)(1-2\nu)}\mathrm{Tr}(\underline{\underline{\varepsilon}})\underline{\underline{I}} \tag{3}$$

with $\underline{\underline{\sigma}}$ the stress tensor, ν the Poisson ratio and E the Young's modulus of the material. One can compute the volumic elastic energy in the material, $\mathrm{d}\mathcal{E}/\mathrm{d}V = (\underline{\underline{\sigma}} : \underline{\underline{\varepsilon}})/2$, which reads,

$$\frac{\mathrm{d}\mathcal{E}}{\mathrm{d}V} = \frac{E}{2(1+\nu)}\left(\underline{\underline{\varepsilon}} : \underline{\underline{\varepsilon}} + \frac{\nu \mathrm{Tr}^2(\underline{\underline{\varepsilon}})}{(1-2\nu)}\right). \tag{4}$$

For a face, $\underline{\underline{\varepsilon}} : \underline{\underline{\varepsilon}} = 2k^2 + k_t^2$ and $\mathrm{Tr}(\underline{\underline{\varepsilon}}) = (2k + k_t)$. The energy of a face reads,

$$\mathcal{E}_{\mathrm{f}} = \frac{Eta^2\left(2k^2 + (1-\nu)k_t^2 + 4\nu k k_t\right)}{2(1+\nu)(1-2\nu)}. \tag{5}$$

Similarly, edge and corner energies read,

$$\mathcal{E}_{\mathrm{e}} = \frac{Eat^2\left(2k_t^2 + (1-\nu)k^2 + 4\nu k k_t\right)}{2(1+\nu)(1-2\nu)} \quad \text{and} \quad \mathcal{E}_{\mathrm{c}} = \frac{3Et^3k_t^2}{2(1-2\nu)}. \tag{6}$$

The elastic energy of a pressurized cell is computed by balancing the energy of face, edge and corner by their number of occurrences divided by their sharing coefficient,

$$\mathcal{E} = \frac{6}{2}\mathcal{E}_{\mathrm{f}} + \frac{12}{4}\mathcal{E}_{\mathrm{e}} + \frac{8}{8}\mathcal{E}_{\mathrm{c}}, \tag{7}$$

The total energy of a cell reads,

$$\mathcal{E} = \frac{3Eta^2}{(1+\nu)(1-2\nu)}\left[\left(1+\frac{1-\nu}{2}\frac{t}{a}\right)k^2 + \left(\frac{1-\nu}{2}+\frac{t}{a}+\frac{1+\nu}{2}\frac{t^2}{a^2}\right)k_t^2 + 2\nu\left(1+\frac{t}{a}\right)kk_t\right] \tag{8}$$

To simplify, the dimensionless energy $\tilde{\mathcal{E}} = \mathcal{E}(1+\nu)(1-2\nu)/3Eta^2$ is considered,

$$\tilde{\mathcal{E}} = \left(1+\frac{1-\nu}{2}\frac{t}{a}\right)k^2 + \left(\frac{1-\nu}{2}+\frac{t}{a}+\frac{1+\nu}{2}\frac{t^2}{a^2}\right)k_t^2 + 2\nu\left(1+\frac{t}{a}\right)kk_t\,. \tag{9}$$

Energy minimization: deformations at equilibrium

Now, the state function of an open system forced by an external pressure is considered. The equilibrium state is given by the minimisation of the function $W = \mathcal{E} - PV$, where PV is the mechanical energy of the fluid. This is an equivalent formulation to the virtual work principle. In dimensionless form, with $\tilde{P} = \dfrac{Pa(1+\nu)(1-2\nu)}{3Et}$, this reads $\tilde{W} = \tilde{\mathcal{E}} - \tilde{P}V/a^3$ with $V = ((1+k)a)^3$ leading to,

$$\tilde{W} = \left(1+\frac{1-\nu}{2}\frac{t}{a}\right)k^2 + \left(\frac{1-\nu}{2}+\frac{t}{a}+\frac{1+\nu}{2}\frac{t^2}{a^2}\right)k_t^2 + 2\nu\left(1+\frac{t}{a}\right)kk_t - \tilde{P}\,(1+k)^3 \tag{10}$$

To simplify the analysis, we suppose that k and $k_t \ll 1$ and thus $\tilde{P} \ll 1$. At the first order the normalised volume reads $1+3k$,

$$\tilde{W} = \left(1+\frac{1-\nu}{2}\frac{t}{a}\right)k^2 + \left(\frac{1-\nu}{2}+\frac{t}{a}+\frac{1+\nu}{2}\frac{t^2}{a^2}\right)k_t^2 + 2\nu\left(1+\frac{t}{a}\right)kk_t - 3\tilde{P}k - \tilde{P} \tag{11}$$

The equilibrium shape is given by the minimization of the function $\tilde{W}$, $\partial\tilde{W}/\partial k = 0$ and $\partial\tilde{W}/\partial k_t = 0$,

$$\begin{cases} \left(2+(1-\nu)\dfrac{t}{a}\right)k + 2\nu\left(1+\dfrac{t}{a}\right)k_t - 3\tilde{P} = 0 \\ \left((1-\nu)+2\dfrac{t}{a}+(1+\nu)\dfrac{t^2}{a^2}\right)k_t + 2\nu\left(1+\dfrac{t}{a}\right)k = 0 \end{cases} \tag{12}$$

One finds

$$\begin{cases} k = 3\dfrac{1-\nu+(1+\nu)\frac{t}{a}}{2(1+\nu)(1-2\nu)+3\frac{t}{a}(1-\nu^2)+(1-\nu^2)\frac{t^2}{a^2}}\tilde{P} \\ k_t = -3\dfrac{2\nu}{2(1+\nu)(1-2\nu)+3\frac{t}{a}(1-\nu^2)+(1-\nu^2)\frac{t^2}{a^2}}\tilde{P} \end{cases} \tag{13}$$

Dimensions on an inflated cell

The relative increase of dimension of an inflated cell are simply given by $\frac{a}{a+t}\left(k+\frac{t}{a}k_t\right)$.

$$\frac{\Delta(a+t)}{a+t} = \frac{3(1-\nu)}{\left(2(1+\nu)(1-2\nu)+3(1-\nu^2)\frac{t}{a}+(1-\nu^2)\frac{t^2}{a^2}\right)}\tilde{P}\,. \tag{14}$$

Thin walls, $t/a \ll 1$	Incompressibility, $\nu \to 1/2$
$k = \dfrac{1-\nu}{2}\dfrac{Pa}{Et}$	$k = \dfrac{3(1-2\nu)(1+3t/a)}{(t/a)^2(3+t/a)}\dfrac{P}{E}$
$k_t = -\nu\dfrac{Pa}{Et}$	$k_t = \dfrac{6(1-2\nu)}{(t/a)^2(3+t/a)}\dfrac{P}{E}$
$\dfrac{\Delta(a+t)}{a+t} = \dfrac{1-\nu}{2}\dfrac{Pa}{Et}$	$\dfrac{\Delta(a+t)}{a+t} = \dfrac{1-2\nu}{(t/a)^2\,(3+t/a)}\dfrac{P}{E}$

Table 3. Deformations in the limit of thin walls and incompressible material from equation (13) and increase of cell dimensions from equation (14).

3.3. Discussion

The predicted stretching k, Equation (13), is drawn in Figure 6 with the parameters corresponding to the prototype 1, see Table 1. The model compares well to experimental data. The model captures both the linear behaviour at small strains and the strains magnitude without fitting parameters. However, the model misses to capture the non-linear behaviour. This artefact may partly be due to the measurement of strains at the free surface and not in bulk material. The pressured cell at the free surface adopts a domed shape with non-uniform deformation, which is not expected in bulk material. Similarly, the strain in the wall is not negative which may also be an artefact of the measurement at the surface and not in bulk material.

When the deformations are larger than 10%, the model fails at predicting the maximal strain. Actually, this is due to two main assumptions made in this modelling, first we considered a Hook's law to describe the elastic material. To take into account very large deformations, hyper-elastic laws should be implemented. Second, we modelled linearised strains which matches the Euler-Lagrange tensor only for small strains. A non-linear treatment of the strains should be done to account for very large deformations. The large strains makes the material softer than for small strains. We thus expect that for large applied pressure, cell deformation may become uneven in the material. This effect is reminiscent of the two-balloon experiment. This effect has been observed experimentally when pressuring the material up to 50 kPa, see figure 8.

Tests were carried out up to very large deformations $\varepsilon \simeq 150\%$ for a pressure of 50 kPa. To keep the prototype intact, larger deformations were not tested. After a strain threshold, the material buckles into a bowl shape (Figure 8). This reversible phenomenon is a first

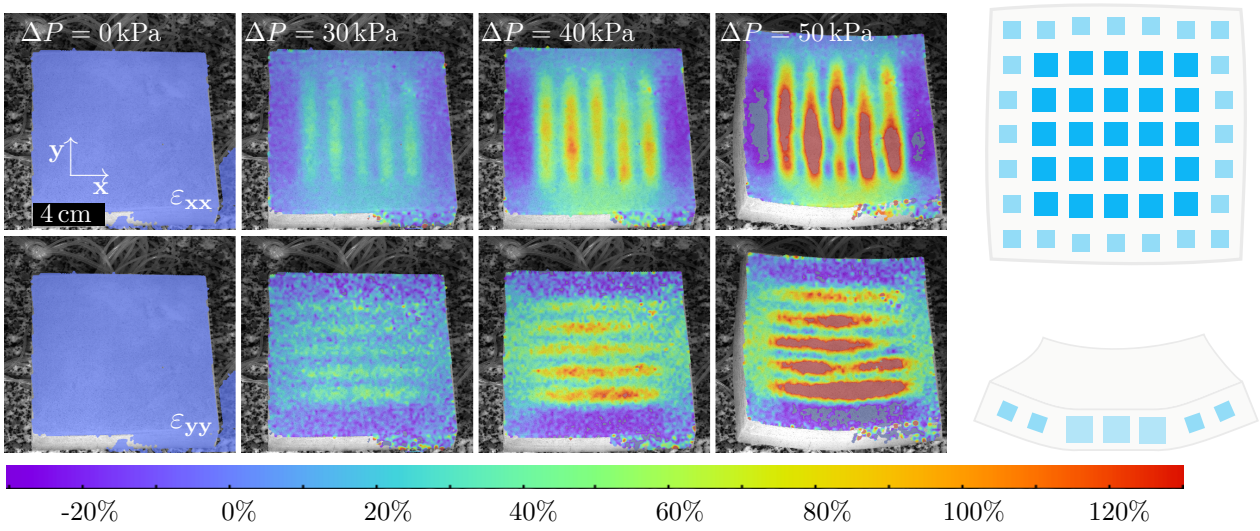

Figure 8. Large deformation of the cellular material. Top: ε_{xx}. Bottom: ε_{yy}. Applied pressure ranges up to 50 kPa. Cellular material edges are stretched in the x-direction for top and bottom which correspond to compression zones for ε_{yy}. Left-right edges behaves inversely. Buckled view of the cellular material (bowl shape).

example of actuation possibility for this cellular material. By superimposition of 2 layers of cellular material, we expect to create on-demand motion without buckling.

The linear anisotropic pattern allowed to create different stains in x and y directions. This strain difference allowed to create an anisotropic stretching of the material. Manual testing of the material also showed that the bending rigidity in both direction was also completely different. This indicates that the macroscopic Young modulus of this cellular material may be controllable by the pressure of the cells.

This simple model of cellular material helps is understanding pulvinus mechanical properties. Currently, cell wall modulus is not well known are values ranging by 3 orders of magnitude have been reported. Cell wall Young modulus of the potato parenchyma has been estimated to $0.5 < E < 0.6$ GPa (Gibson 2012). Values of $0.3 < E < 0.7$ MPa have also been used in the modelling of Mimosa Pudica (Wang & Li 2020). Considering the dimensions of pulvinus cells at rest and pressured (a_{rest}=25 µm, a_{press}=45 µm), one computes a stretching $k = 1 - a_{\text{rest}}/a_{\text{press}} \simeq 44\%$. Inverting the strain for thin wall (Table 3), one finds,

$$E = \frac{1-\nu}{2}\frac{Pa}{kt}. \tag{15}$$

Considering typical values for Mimosa Pudica, cell wall thickness t=1 µm, parenchyma cell wall poisson ratio ν=0.3, and typical turgor pressure of P=1 MPa, one computes the expected cell wall Young modulus, $E \simeq 24$ MPa.

The actuation stress in the material depends on the applied pressure to cells, ΔP. To

be more specific, one may consider a simple hook experiment where a rectangular cuboid of cellular material has an initial section S_0, Young modulus E_0, length L_0 and produces no force when not pressurised. When increasing the pressure at fixed length, the surface of the material expands by $\varepsilon \propto \Delta P^2$, Equation (14). The force exerted by the f is simply the surface of cells time pressure $f = \Delta P S \propto \Delta P^3$. The actuation stress is then given by the Hook's law, $\varepsilon = f/E_0 S \propto \Delta P/E_0$. The actuation stress may be roughly estimated as the applied pressure to the cells. However, as the pressure increases, the material may stiffen linearly with pressure (Nilsson et al. 1958) which would involve a sub-linear increase of the actuation stress, possibly reaching a plateau.

Another possible biomimetic aspect of pulvinus is to mimic its structure to create resilient actuators. Little attention has been paid on the resilience of pulvinus that even amputated by a half, continues performing complex motions (Millet et al. 1989). Considering resilience as the ability to preserve performances when damaged most of the works on bio-inspired resilience has been done on the control chain (software) where biological laws of adaptation have been mimicked to adapt a complex robot to a deficient unit (Cully et al. 2015). We hope that the development of multi-cellular actuator inspired by pulvinus may help in creating resilient actuators with the capacity to produce on-demand mechanical properties and on-demand complex motions.

4. Conclusion

The developed prototype of cellular material is the first controllable material at the cell level. The deformations of the material when pressurized indicate zones of stretching (along the faces) and zones of compression (perpendicularly to faces).

The modelling proposed in the present paper explains the material behaviour at small strains but fails in describing very large strains. Very large strains may be useful to create large-stroke versatile actuators. Next efforts should be done to understand the material behaviour when highly pressurized.

The next steps include (i) changing the pressurization pattern to create on-demand macroscopic mechanical properties, (ii) analyse the possibility of motion depending on inflation (isotropic growth, anisotropic expansion and buckling) and (iii) create larger array of cells, possibly 3D.

Bibliography

APG IV T 2016 *Botanical journal of the Linnean Society* **181**(1), 1–20.
Boonvisut P & Çavuşoğlu M C 2012 *IEEE/ASME Transactions on Mechatronics* **18**(5), 1602–1611.

Cota-Sánchez J H, Almeida O J, Falconer D J, Choi H J & Bevan L 2013 *Flora-Morphology, Distribution, Functional Ecology of Plants* **208**(5-6), 381–389.

Cully A, Clune J, Tarapore D & Mouret J B 2015 *Nature* **521**(7553), 503–507.

Dumais J & Forterre Y 2012 *Annual Review of Fluid Mechanics* **44**, 453–478.

Fleurat-Lessard P & Millet B 1984 *Journal of Experimental Botany* **35**(9), 1332–1341.

Forterre Y 2013 *Journal of experimental botany* **64**(15), 4745–4760.

Gibson L J 2012 *Journal of the royal society interface* **9**(76), 2749–2766.

Gurstelle W 2017 *ReMaking History, Volume 3: Makers of the modern world* Maker Media, Inc.

Hannaford B & Winters J 1990 *in* 'Multiple muscle systems' Springer pp. 101–120.

Higueras-Ruiz D R, Nishikawa K, Feigenbaum H & Shafer M 2021 *Bioinspiration & biomimetics* .

Li S & Wang K 2015*a* *Smart Materials and Structures* **24**(10), 105031.

Li S & Wang K 2015*b* *Journal of The Royal Society Interface* **12**(111), 20150639.

Li S & Wang K 2016 *Bioinspiration & biomimetics* **12**(1), 011001.

Millet B, Coillot L & Agosti R D 1989 *Plant and cell physiology* **30**(5), 643–648.

Morin A H 1951 *1.003.449* .

Morin A H 1953 *US2642091 Patent* .

Must I, Sinibaldi E & Mazzolai B 2019 *Nature communications* **10**(1), 1–8.

Nilsson S B, Hertz C H & Falk S 1958 *Physiologia Plantarum* **11**(4), 818–837.

Piyasena M E, Newby R, Miller T J, Shapiro B & Smela E 2009 *Sensors and Actuators B: Chemical* **141**(1), 263–269.

Shepherd R F, Ilievski F, Choi W, Morin S A, Stokes A A, Mazzeo A D, Chen X, Wang M & Whitesides G M 2011 *Proceedings of the national academy of sciences* **108**(51), 20400–20403.

Siéfert E, Reyssat E, Bico J & Roman B 2019 *Nature materials* **18**(1), 24–28.

Vasista S & Tong L 2012 *AIAA journal* **50**(6), 1328–1338.

Villegas D, Van Damme M, Vanderborght B, Beyl P & Lefeber D 2012 *Advanced Robotics* **26**(11-12), 1205–1227.

Wang Y & Li H 2020 *Bioelectrochemistry* **134**, 107533.

Xu Z, Zhou Y, Zhang B, Zhang C, Wang J & Wang Z 2021 *Micromachines* **12**(6), 608.

Zhang J, Sheng J, O'Neill C T, Walsh C J, Wood R J, Ryu J H, Desai J P & Yip M C 2019 *IEEE Transactions on Robotics* **35**(3), 761–781.